HAL
open science

Evidence of Band Bending Induced by Hole Trapping at MAPbI3 Perovskite / Metal Interface

Yan Fang Chen, Yan T Tsai, Dario Bassani, Raphael Clerc, D Forgács, H J Bolink, W Wussler, J J Jaegermann, G Wantz, L Hirsch

To cite this version:

Yan Fang Chen, Yan T Tsai, Dario Bassani, Raphael Clerc, D Forgács, et al.. Evidence of Band Bending Induced by Hole Trapping at MAPbI3 Perovskite / Metal Interface. Journal of Materials Chemistry A, 2016, 10.1039/C6TA08979H . hal-01388229

HAL Id: hal-01388229

https://hal.science/hal-01388229v1

Submitted on 26 Oct 2016

HAL is a multi-disciplinary open access archive for the deposit and dissemination of scientific research documents, whether they are published or not. The documents may come from teaching and research institutions in France or abroad, or from public or private research centers.

L'archive ouverte pluridisciplinaire **HAL**, est destinée au dépôt et à la diffusion de documents scientifiques de niveau recherche, publiés ou non, émanant des établissements d'enseignement et de recherche français ou étrangers, des laboratoires publics ou privés.

View Article Online
View Journal

Journal of
Materials Chemistry A

Accepted Manuscript

This article can be cited before page numbers have been issued, to do this please use: Y. Chen, Y. Tsai, D. Bassani, R. Clerc, D. Forgács, H. J. Bolink, M. Wussler, W. Jaegermann, G. Wantz and L. Hirsch, *J. Mater. Chem. A*, 2016, DOI: 10.1039/C6TA08979H.

This is an *Accepted Manuscript*, which has been through the Royal Society of Chemistry peer review process and has been accepted for publication.

Accepted Manuscripts are published online shortly after acceptance, before technical editing, formatting and proof reading. Using this free service, authors can make their results available to the community, in citable form, before we publish the edited article. We will replace this *Accepted Manuscript* with the edited and formatted *Advance Article* as soon as it is available.

You can find more information about *Accepted Manuscripts* in the Information for Authors.

Please note that technical editing may introduce minor changes to the text and/or graphics, which may alter content. The journal's standard Terms & Conditions and the Ethical guidelines still apply. In no event shall the Royal Society of Chemistry be held responsible for any errors or omissions in this *Accepted Manuscript* or any consequences arising from the use of any information it contains.

ROYAL SOCIETY OF CHEMISTRY

www.rsc.org/materialsA

View Article Online
DOI: 10.1039/C6TA08979H

Journal of Materials Chemistry A

ARTICLE

Published on 26 October 2016. Downloaded by UNIVERSITE DE BORDEAUX on 26/10/2016 14:41:41.

Journal of Materials Chemistry A Accepted Manuscript

Evidence of Band Bending Induced by Hole Trapping at $MAPbI_3$ Perovskite/Metal Interface

Received 00th January 20xx,
Accepted 00th January 20xx

DOI: 10.1039/x0xx00000x

www.rsc.org/

Y.-F. Chen [a,b], *Y.-T. Tsai* [a,b], *D. M. Bassani* [b], *R. Clerc* [c]†, *D. Forgács* [d], *H. J. Bolink* [d], *M. Wussler* [e], *W. Jaegermann* [e], *G. Wantz* [a], *and L. Hirsch*,[a]*

Electron injection by tunneling from a gold electrode and hole transport properties in polycrystalline $MAPbI_3$ has been investigated using variable temperature experiments and numerical simulations. The presence of a large and unexpected band bending at the Au/$MAPbI_3$ interface is revealed and attributed to the trapping of holes, which enhances the injection of electrons via tunneling. These results elucidate the role of volume and interface defects in state-of-the-art hybrid perovskite semiconductors.

Introduction

Hybrid organic–inorganic perovskite (HOIP) based solar cells represent an attractive technology that features record power conversion efficiency (PCE) in constant increase. This success story started in 2009 with the report by Kojima et al. of a HOIP solar cell with 3.8% PCE.[1] In 2016, the current PCE record obtained by Saliba et al. is 21.1 %.[2] The progression of perovskite solar cell PCE is the fastest for all types of solar cell technology. This class of materials benefits from preexisting knowledge of both inorganic semiconductors (charge transport, band structure) and organic semiconductors (wet process, soft substrates, etc.). Nevertheless, the spread of PCE found in literature is still very large, suggesting that material properties and interfaces remain very dependent on the fabrication process. The polycrystalline nature of the active layer thus gives rise to grain boundary defects which add to the bulk crystallographic defects. Using numerical simulations, Yin et al.[3] have shown that defects with low formation energies create only shallow traps, whereas defects with deep levels require high formation energies. In other words, formation of deep trap states is likely to be rather limited in HOIPs, leading to the observation of long charge carrier lifetimes,[4] and low Urbach tail energy.[5] These exceptional electrical properties are clearly one of the advantages of HOIPs for solar cell applications.

Despite numerous investigations, the role of trapping is still under debate and recent studies report trap density as high as 10^{16}–10^{17} cm^{-3}, as determined by photoluminescence quenching or steady state PL intensity.[6,7] Wu et al. remarked that trap density are augmented at surfaces and interfaces where the perovskite crystal structure is most susceptible to deformation.[8] In their study, they have proven the presence of a broad distribution of hole traps at the surface of the $CH_3NH_3PbI_3$ perovskite thin film. A recent review by Brenner et al. also highlights that numerous intrinsic parameters still need to be refined, and that future work should also consider temperature effects as well as the role of grain boundaries and material interfaces on defect formation.[9] From this, it emerges that surfaces and interfaces play a crucial role in the operation of lead iodide perovskite based devices. In this context, the aim of this work is to investigate the metal/HOIP interface by exploiting the injection of electrons by tunneling, allowing us to probe the nature of the barrier at this interface. Because the tunneling injection mechanism is strongly dependent on the barrier height and thickness,[10] this approach is extremely sensitive to the nature of the interface including, for example, modification of the barrier height induced by a local electric field due to doping or trapping at the metal/HOIP interface.

[a] University of Bordeaux, IMS, UMR 5218, F-33400 Talence, France and CNRS, IMS, UMR 5218, F-33400 Talence, France.
[b] Institute of Molecular Sciences. University of Bordeaux CNRS UMR 5255, Bâtiment A12, 351 Cours de la libération, 33405 Talence Cedex, France..
[c] Institut d'Optique Graduate School. Université de Lyon, UJM-Saint-Etienne CNRS UMR 5516, Laboratoire Hubert Curien, 42023 Saint-Etienne, France
[d] Instituto de Ciencia Molecular. Universidad de Valencia Calle Cat. J. Beltran 2, 46980 Paterna, Spain
[e] Surface Science Division, Institute of Materials Science, Darmstadt University of Technology Petersenstr. 32, 64287 Darmstadt, Germany
† Email: raphael.clerc@institutoptique.fr
* E-mail: lionel.hirsch@ims-bordeaux.fr
Electronic Supplementary Information (ESI) available: details of any supplementary information available should be included here. See DOI: 10.1039/x0xx00000x

Please do not adjust margins

View Article Online
DOI: 10.1039/C6TA08979H

Published on 26 October 2016. Downloaded by UNIVERSITE DE BORDEAUX on 26/10/2016 14:41:41.

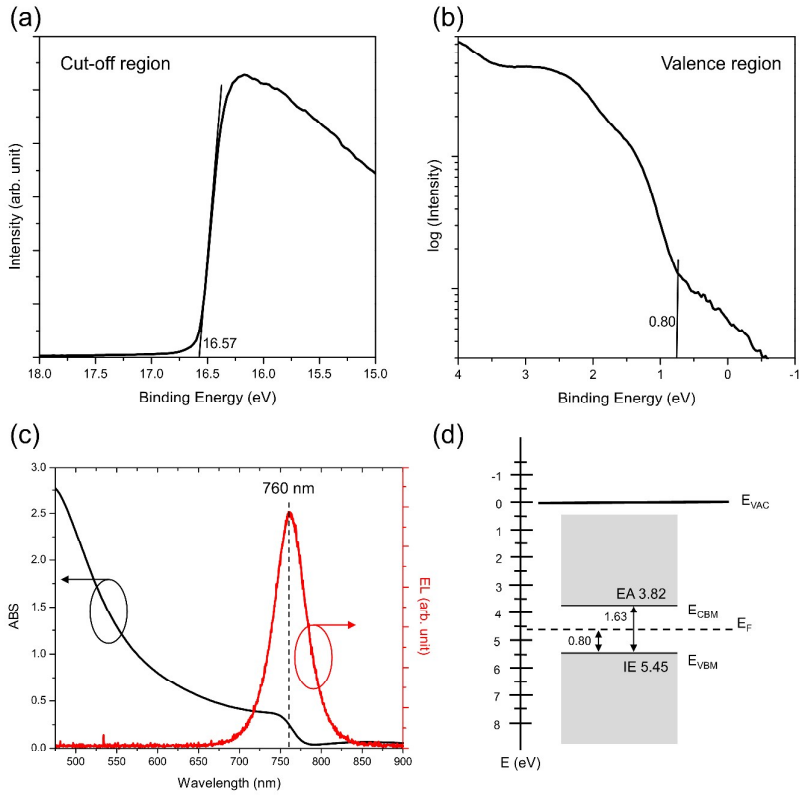

Figure 1: **UPS spectrum of ITO/PEDOT:PSS/$MAPbI_3$ (300 nm) at (a) the cut-off region and (b) the valence region. To determine the valence band maximum, the valence region is displayed in logarithmic scale.[11] The Fermi level and the ionization potential can be derived from the intercepts shown in the graphs. (c) The absorption and electroluminescence spectra of $MAPbI_3$ film. The electroluminescence was recorded from ITO/PEDOT:PSS/$MAPbI_3$ (300 nm)/$PC_{61}BM$/Ca/Al. (d) Summary of the determined energy levels of $MAPbI_3$. The Fermi level is almost in the middle of the bandgap**

Tunneling injection depends on the energetics of the barrier as well as on the effective mass of the particle that is tunneling. Several groups reported theoretical values of this important parameter, but to date the only two experimentally determined values were obtained by Miyata et al. using magneto-absorption technique,[12] and by Price et al. using a band-filling model to fit transient absorption spectroscopy data.[13] Their finding gave values of $m^* \approx 0.1–0.14\ m_0$ ($m_0 \approx 9.1\times10^{-31}$ kg is the free electron mass). From the theoretical values reported in literature although one can clearly observe discrepancies between the various reports, the majority of the values cluster at $m^* \approx 0.2\ m_0$,[14,15,16,17] but Feng et al. found values between 0.76 and 2.65 m_0,[18] and Motta et al. values between 0.03 and 0.5 m_0.[19] Therefore, it should be possible in theory to independently confirm m^* from the tunneling electron injection experiments, provided that the metal/HOIP interface is ideal, i.e. without defects. In case of a non-ideal metal/HOIP interface, the nature of the barrier, potentially impacted by band bending, can be investigated by tunneling injection experiments, however at the cost of assuming a value for m^*.

Herein, we report an in-depth investigation of the interfacial trap densities and how these affect band bending in a typical HOIP device optimized for electron injection via tunneling. A gold electrode was selected in order to maximize the electron barrier height for tunneling both current and luminance intensity were recorded to discriminate electron from hole injection. Surprisingly, the results are consistent with a material possessing a very low doping level, but in which the presence of hole traps results in the appearance of significant band bending under standard operating conditions.

Results and discussion

In order to determine the schematic band diagram of $MaPbI_3$ perovskite, UPS, UV-Vis absorption and electroluminescence data are required. The optical bandgap was determined by UV/vis absorption and by electroluminescence spectra. Earlier reports suggest that the exciton binding energy in $MAPbI_3$ is less than 60 meV,[20,21] and Miyata et al.[12] have recently shown that the value can be as low as 16 ± 2 meV, indicating that the optical bandgap can be assumed equal to the electronic bandgap. The structure of the solar cell used for electroluminescence characterization was ITO/PEDOT:PSS/$MAPbI_3$/$PC_{61}BM$/Ca/Al. Maximum emission is recorded at 760 nm (1.63 eV), in agreement with band-edge absorption as shown in Figure 1. Finally, we

Journal of Materials Chemistry A Accepted Manuscript

Please do not adjust margins

View Article Online
DOI: 10.1039/C6TA08979H

Published on 26 October 2016. Downloaded by UNIVERSITE DE BORDEAUX on 26/10/2016 14:41:41.

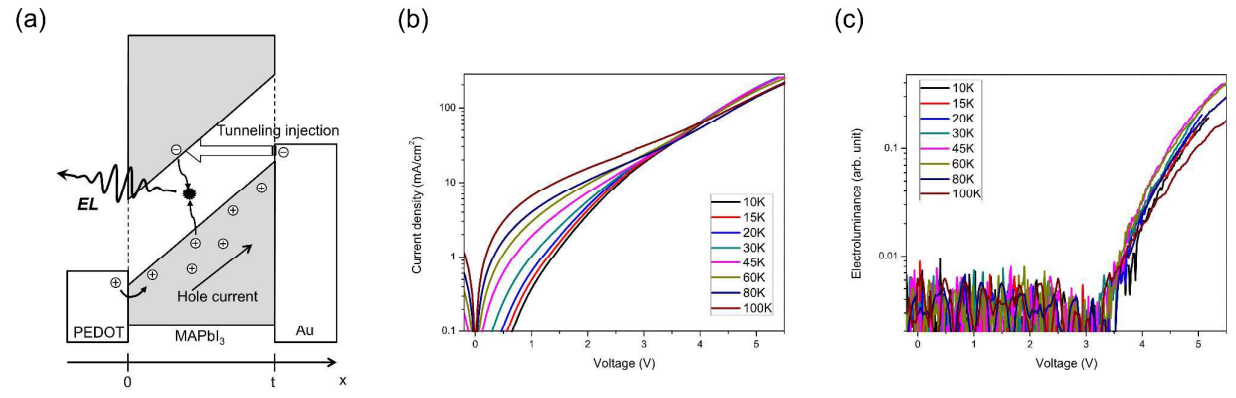

Figure 2: **(a) Working principle scheme of the experiment. Electrons are injected through $MAPbI_3$/Au contact by tunneling and recombine with holes from bottom electrode in $MAPbI_3$ layer. (b) Current and (c) luminance versus voltage as function of temperature of ITO/PEDOT:PSS/$MAPbI_3$ (200nm)/Au device. The EL signals are invariant with respect to temperature, supporting the tunneling injection mechanism**

determined the ionization potential (IP = 5.59 eV) and the work function (WF = 4.65 eV) of the lead iodide perovskite material using UPS. The Fermi level is almost in the middle of the bandgap as shown in Figure 1. This indicates that residual doping is low, confirming that the $MAPbI_3$ layer is stoichiometric. This is also consistent with the theoretical work of Yin et al.[3] on the defect formation energies. Then, as shown in Figure 1, it is possible to deduce the theoretical metal/$MAPbI_3$ barrier height, defined as the difference between the metal work function and the $MAPbI_3$ electron affinity. For electrons, the barrier height between the gold electrode and the $MAPbI_3$ semiconductor should be equal to 1.28 eV if we consider a gold work function of 5.1 eV and the $MAPbI_3$ electron affinity to be 3.82 eV. For holes, the barrier is expected to be much lower, in the range of 0.4 eV. In such a device architecture, the injections of electrons and holes in the direct regime is highly asymmetrical, rendering the electron current negligible compared to the hole current. Because radiative recombination requires both electron and holes, it is safe to assume that the recombination rate is limited by the electron current.

According to the electron continuity equation:

$$j_n(t) - j_n(0) = \int_0^t eR(x)dx \qquad (1)$$

where $R(x)$ is the radiative recombination rate and j_n the electron current density. Assuming that electrons are injected at $x = t$ (see Figure 2), and that the concentration of holes injected is much higher than the one of electrons ($j_n(0) << j_n(t)$), we may simplify the electron current density to be:

$$j_n(t) \approx \int_0^t eR(x)dx \qquad (2)$$

In other words, the light intensity measured in the current and luminance versus voltage (IVL) experiments can be assumed to be proportional to the injected current density of electrons though the ~ 1eV barrier. Electroluminescence (EL) was measured simultaneously with the current as shown in Figure 2. The presence of both charge carriers in the $MAPbI_3$ layer is confirmed by the electroluminescence signal, which is assumed to be limited by the minority charge carrier injection. Then, the EL signal can be used to measure the electron injection (when a gold cathode is used). Relative intensities recorded at different temperatures are comparable since the geometry is fixed and the photodetector operates in the linear regime, far from saturation. However, because only a fraction of the photons produced by spontaneous emission can be collected, the value of the proportionality constant between the electron injection current j_n and the measured photocurrent is not known.

The quality of the $MAPbI_3$ perovskite used in these studies was evaluated using X-ray diffraction (XRD), photoemission spectroscopies (XPS and UPS), atomic force microscopy, and from the performance of solar cells fabricated with this material. XRD spectra show that the deposited layer is polycrystalline and neither amorphous areas nor residual PbI_2 were detected in the diffractograms (See supplementary information, Figure S1). XPS results confirm

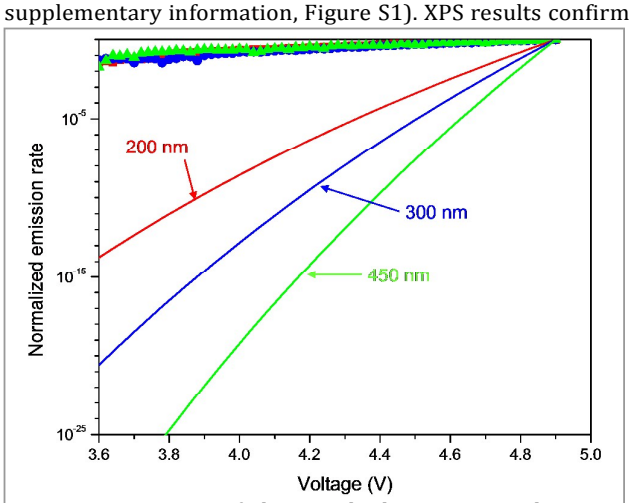

Figure 3: **Comparison of the normalized emission rate between simulations assuming Fowler–Nordheim tunneling through a triangular barrier (lines) and experimental data (dots) with $MAPbI_3$ thickness 200 nm, 300 nm and 450 nm. The experimental data at 10 K are used. In all 3 cases, the simulated rates are much lower than the experimental data.**

Journal of Materials Chemistry A Accepted Manuscript

Please do not adjust margins

View Article Online
DOI: 10.1039/C6TA08979H

Published on 26 October 2016. Downloaded by UNIVERSITE DE BORDEAUX on 26/10/2016 14:41:41.

that only the expected elements are present in the lead iodide perovskite layer (Figure S2). $CH_3NH_3PbI_3$ perovskite solar cells with ITO/PEDOT:PSS/$MAPbI_3$ (200nm)/$PC_{61}BM$ (50nm)/Ca/Al were prepared and characterized. About 90 samples have been processed and average power conversion efficiency has been found equal to 11.2% ± 1.4% (Figure S3, Supporting Information) with typical J_{sc} = 22.6 mA cm^{-2} ; V_{oc} = 0.73 V and FF = 0.78 (Figure S4, Supporting Information). All these results are consistent with most of those reported in literature.[22,23,24] Some samples had record efficiencies over 15% that is close to the state-of-the-art for this device architecture.[25,26] In conclusion, the process used in this work is representative of typical results obtained using $MAPbI_3$ material.

Typical variable temperature $I(V)$ data are shown in Figure 2. Two regimes on the $I(V)$ curves can be observed: at low voltage, the current is thermally activated, whereas at higher voltage, the current is almost temperature independent. This second regime is typical of tunneling injection and it coincides with the onset of electroluminescence, in agreement with the hypothesis that injection of electrons across the gold cathode is the limiting phenomenon for electroluminescence. Therefore, at low temperatures, electron injection occurs via tunneling and should obey the Fowler–Nordheim (FN) relationship governing tunneling through a triangular barrier.

A comparison between normalized simulations of Fowler–Nordheim tunneling currents with experimental normalized emission rate is reported on Figure 3. In the simulation, the electron effective mass has been taken equal to 0.2 m_0 (which correspond to an average value of the reported electron conduction band effective mass) and the dielectric constant to be ε_r = 30 (obtained from the $C(V)$ measurements at 0 V, 10 kHz). Clearly, the fit between the simulated data and the experimental observations is very poor. As expected, FN currents exhibit a strong voltage and thickness dependency, which is however almost absent in the experiments. Further refinement of the FN model does not improve the quality of the fit. For example, the inclusion of image force lowering or the introduction of a 2 band Franz dispersion relation provides no significant improvement,[27] essentially because of the high value of the perovskite dielectric constant. Only an unrealistically low value of the tunneling effective mass, m^* < 0.01 m_0 improves the comparison between the experiment results and the FN simulations. Moreover, it has to be noted that the electron current in the approximation of tunneling through a triangular barrier is calculated to be extremely low, meaning that light emission should negligible. All these observations suggest the existence of a mechanism that is enhancing the injection of electron by tunneling. Significant band bending at the Au/$MAPbI_3$ interface would explain both the increase of electron tunneling injection as well as the almost thickness independence of the luminance versus voltage curves.

Band bending is often the consequence of the formation of a depletion layer induced by residual doping. However, this hypothesis is highly unlikely in the present case. Indeed, contrary to a typical Schottky diode, capacitance versus voltage experiments (Figure 4) are flat around 0 V. This result clearly demonstrates that no band bending exists under short circuit conditions as expected for an undoped semiconductor. This is further emphasized by the UPS results presented in Figure 1 which show that the Fermi level is close to the middle of the bandgap, as is the case for non-intentionally doped material. Another possible explanation for the occurrence of band bending at the interface would be the accumulation of ions in a non-doped material. Such ionic transport is well known in perovskites, but it is highly temperature dependent and unlikely at low temperatures. Indeed, we observe ion mobility effects in the $C(V)$ experiments at room temperature, but they disappear

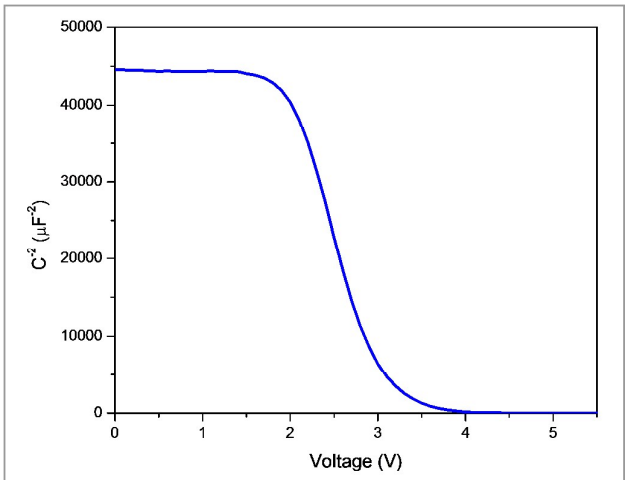

Figure 4: **The Mott-Schottky plot of ITO/PEDOT:PSS/$MAPbI_3$ (300 nm)/Au. The zero slope near 0 V indicates the absence of intrinsic doping. Data recorded at 10 kHz with alternating voltage of 30 mV. The sample temperature was 15K.**

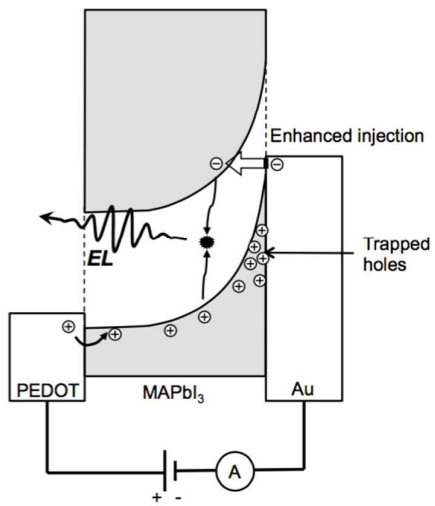

Figure 5: **Schematic view of the expected band structure of the ITO/PEDOT:PSS/$MAPbI_3$/Au device, assuming a space charge effect band curvature induced by trapped holes at the $MAPbI_3$/Au interface.**

Journal of Materials Chemistry A Accepted Manuscript

Please do not adjust margins

View Article Online
DOI: 10.1039/C6TA08979H

Published on 26 October 2016. Downloaded by UNIVERSITE DE BORDEAUX on 26/10/2016 14:41:41.

immediately as soon as the temperature is lowered. In front of this paradox, the assumption of the existence of an unexpected space charge effect has to be considered. The explication proposed in this work is that this band bending is in fact induced by the trapping of holes near the Au/$MAPbI_3$ interface. In the following, we demonstrate by comparison with simulation that this assumption is consistent with both the experimental electroluminescence and current measurements for all device thicknesses.

As one can see in Figure 1b, a band tail of states is present in the bandgap above the valence energy. These states can trap holes once injected in the $MaPbI_3$ layer shifting the Fermi energy toward the valence energy. One can thus assume that a large concentration of hole traps are localized in vicinity of the Au contact. To simplify the calculation, the energy level of these traps is assumed to be close to the valence band, and the traps are charged only when occupied by a hole. In the high voltage regime where emission is measured, it is reasonable to assume that all these traps are filled, leading to an important positive charge localized close to the $MAPbI_3$/Au interface as shown in Figure 5. In order to test this assumption, the following model has been proposed. First of all, the hole trap concentration is set equal to:

$$N_T(x) = N_{T1} + N_{T2}\exp\left(\frac{t-x}{\lambda}\right) \quad (3)$$

where t is the $MAPbI_3$ thickness, N_{T1} the volume trap concentration and N_{T2} the perovskite/Au interface trap concentration x = t. Eq. 3 essentially states that the concentration of hole traps exponentially increases in a region localized at few λ from the $MAPbI_3$/Au interface. The electrostatic potential can be deduced for the trap concentration by solving the Poisson equation, with the following boundary conditions V(x = 0) = –Va, V(x = t) = 0, leading to:

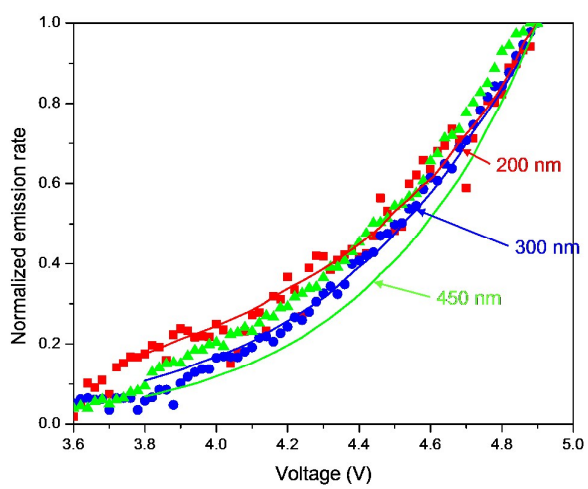

Figure 6: **Comparison between normalized tunneling current simulations (lines) considering a strong space charge effect at the MAPbI3/Au interface. (thickness 200 nm, 300 nm and 450 nm) and corresponding experimental normalized emission rate at 10 K (symbols).**

$$V(x) = V_a\left(\frac{x}{t} - 1\right) + \frac{eN_{T1}}{2\varepsilon}(x^2 - tx) + \frac{eN_{T2}\lambda^2}{\varepsilon}\left[\exp\left(-\frac{t-x}{\lambda}\right) - \exp\left(-\frac{t}{\lambda}\right)\left(1 - \frac{x}{t}\right) - \frac{x}{t}\right] \quad (4)$$

Once knowing the band curvature, the electron tunneling current can be numerically calculated using the following formulae:

$$J(V_a) = \frac{4\pi m e^2 kT}{h^3}\int_0^\infty T(E,V_a)\ln\left(1 + \exp\left(\frac{E-E_F}{kT}\right)\right)dE \quad (5)$$

where $T(E,V_a)$ is the tunnel transparency calculated using the Wentzel–Kramers–Brillouin (WKB) approximation and the electron tunneling mass is 0.2 m_0. This latter is given by:

$$T(E,V_a) = \exp\left[-2\int_0^{a(E)}\sqrt{\frac{2m(\phi - eV(x) - E)}{\hbar^2}}dx\right] \quad (6)$$

where E_p is the potential energy (band curvature), related to the $MAPbI_3$ /Au interface barrier height ϕ and the electrostatical potential V(x) by

$$E_p(x,V_a) = \phi - eV(x,V_a) \quad (7)$$

Both the trap concentration (Figures S5 and S6, Eq(3)) and the corresponding band curvature Eq(7) illustrate the impact of localized high trap concentrations at the $MAPbI_3$/Au interface on the tunneling barrier.

Concerning the emission rate experiments, as seen in Figure 6, a much better agreement between experiments and simulations is obtained, allowing one to extract $\lambda \sim 6.5$ nm and $N_{T2} \sim 5.5\ 10^{19}$ cm^{-3} (N_{T1} has little impact on the tunneling current, and has been estimated from the *I-V* curves as explained below). The corresponding charge density $q\ N_{T2}\ \lambda$ is high, in the range of ~ 0.055 C/m^2. The assumption of a uniform volume trap density has also been considered ($N_T(x) = N_T$). However, in this case, the model would predict a stronger thickness and voltage dependence, which is not compatible with the experimental data. This further confirms the assumption of equation (3) concerning the "localized" trapping of holes at the $MAPbI_3$ / Au interface.

The *I–V* curves are simulated considering only hole transport as the electron current remains negligible, especially for an applied voltage lower than 3 V. Therefore, the model is essentially a space charge limited current (diffusion has been neglected) in presence of both volume and interface hole traps.[28]

The incomplete filling of traps along the device has been considered. For simplicity, in order to limit the number of fitting parameters, only one energy level of traps are included (the same energy level for both volume and interface traps). The corresponding system of equations is:

$$j = e\,\mu\,p\,E \quad (8)$$

$$\frac{dE}{dx} = \frac{e}{\varepsilon}\left[p + \frac{p}{p+p_1}N_T(x)\right] \quad (9)$$

$$V = \int_0^t -E(x)dx \quad (10)$$

As the right-end side of equation (8) depends both on p and x, it is not possible to find a closed form solution for all

Journal of Materials Chemistry A Accepted Manuscript

Please do not adjust margins

View Article Online
DOI: 10.1039/C6TA08979H

Published on 26 October 2016. Downloaded by UNIVERSITE DE BORDEAUX on 26/10/2016 14:41:41.

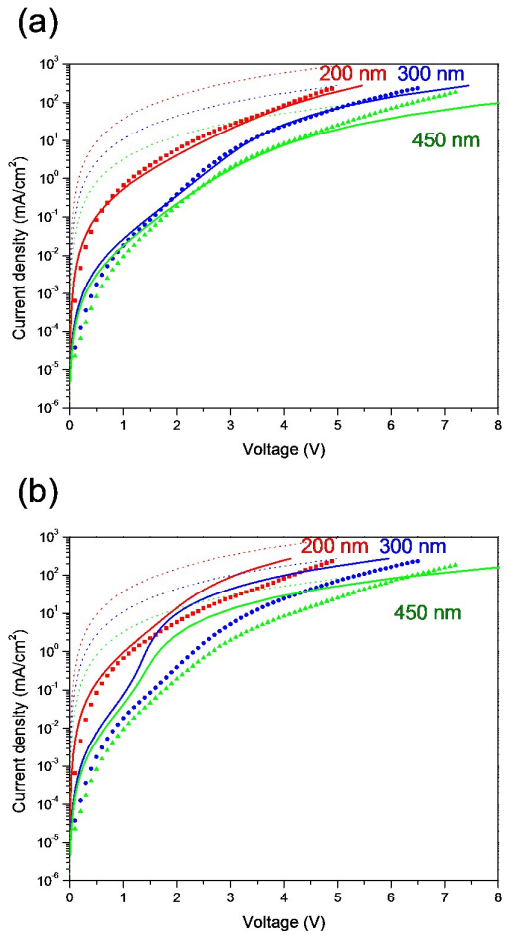

Figure 7: **Simulation of current–voltage characteristics at 10K of ITO/PEDOT:PSS/$MAPbI_3$/Au with active layer thickness 200, 300, and 450 nm. (a) Full model including volume and interface traps. (b) Model with volume trap only. Models are the solid lines, experimental data symbols. Dot line represent pure SCLC model with no traps. Fitting parameters are presented in Table 1.**

voltages. Equations (8–10) have thus been solved numerically. In this approach, the unknown parameters are the mobility μ, N_{T1} and p_1, which are obtained by fitting (see results Table 1). N_{T2} and λ were not considered as fitting parameters because they have been determined previously from the emission experiments for all devices. It is not possible to keep the same trap parameters N_{T1} and p_1 for all the devices (featuring different thicknesses), but this seems reasonable in view of some moderate variability. Nevertheless, as seen Table 1, the N_{T1} and p_1 variation remains reasonable enough to validate this approach.

Finally, the energy trap levels can be deduced from p_1 using the following equation:

$$p_1 = N_v(T)\exp(\frac{-E_T}{kT}) \quad (9)$$

with $N_v(T) \propto T^{3/2}$ and N_v(300K) = 1.8 × 10^{19} cm^{-3} according to Minemoto and Murata.[29]

Table 1: **Fitting parameters for current–voltage curves presented in** Figure 7.

Sample thickness nm	200	300	450
Mobility $cm^2 V^{-1}s^{-1}$		10^{-4}	
N_{T2} cm^{-3}		5.5×10^{19}	
λ nm		6.5	
N_{T1} cm^{-3}	1.6×10^{17}	5×10^{16}	2.3×10^{16}
p_1 cm^{-3}	2×10^{15}	8×10^{13}	8×10^{13}
E_T meV	3.7	6	6

Simulations and experiments therefore show an overall good agreement, as illustrated in Figure 7. Furthermore, it can be seen that neither simple SCLC (neglecting all traps), nor the SCLC model with constant volume trap density, can reproduce the experimental results. Only a model including the trap density given by equation (3) can correctly fit the experiments, which further confirms the existence of enhanced trapping at the $MAPbI_3$/Au interface.

Interestingly, the value of the volume trap density found in this work is in good agreement with previous studies.[6,7] Similarly, the value of E_T obtained (3.7–6 meV) is consistent with calculations by Yin et al.[3] Also, we would like to emphasize that the value of E_T obtained is coherent with the rapid hole release at 10K when the device is short-circuited. It is also important to note that the extracted charge carrier mobility has a surprisingly low value (~10^{-4} $cm^2 V^{-1} s^{-1}$ at high field), which is however plausible in a disordered medium such as polycrystalline $MAPbI_3$ at low temperatures. In the literature, reported charge carrier mobility values vary over a large range (between 10 $cm^2 V^{-1} s^{-1}$ and 10^{-4} $cm^2 V^{-1} s^{-1}$),[30,31,32] presumably due to different material processes and experimental techniques. The highest values are obtained on single crystals using THz spectroscopy, whereas the lower values are typical of polycrystalline materials. In order to assess the charge carrier mobility at low temperature, we carried out time of flight (TOF) experiments on a device with structure ITO/PEDOT:PSS/$MAPbI_3$ (300 nm)/Au. The results are shown in Figure 8, where the mobility obtained is given as a function of temperature. Although a modest temperature dependence is observed, the TOF mobility is indeed found to be ca. 10^{-4} $cm^2 V^{-1} s^{-1}$.

Experimental

Thin film preparation: The ITO-covered glass substrates (ITO thickness 150 nm, resistivity ~15 Ω sq^{-1} supplied by *Visiontek*) were cleaned by successive sonication in acetone, ethanol, and isopropyl alcohol (15 minutes each), followed by UV-Ozone treatment for 10 minutes. Poly(3,4-ethylenedioxythiophene) polystyrene sulfonate

Journal of Materials Chemistry A Accepted Manuscript

Please do not adjust margins

View Article Online
DOI: 10.1039/C6TA08979H

Published on 26 October 2016. Downloaded by UNIVERSITE DE BORDEAUX on 26/10/2016 14:41:41.

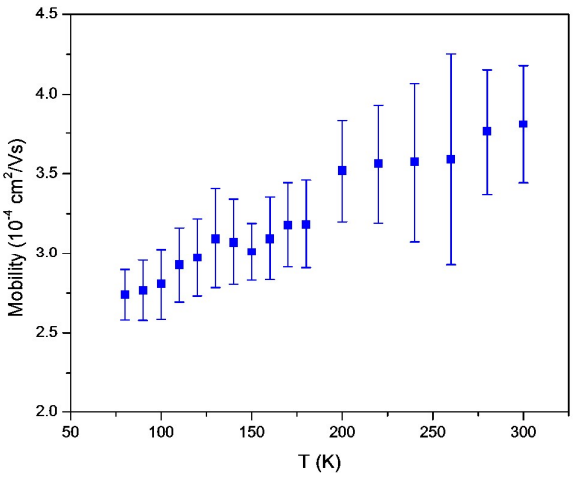

Figure 8: **The temperature dependence of MAPbI3 hole mobility using time of flight measurement. An bias of −3 V was applied on ITO/PEDOT:PSS/MAPbI3 (300 nm)/Au to separate the photogenerated electron−hole pairs. The time of flight photocurrent is shown in Figure S3.**

(PEDOT:PSS, *Heraeus, Clevios-PH*) was spin coated onto the clean substrates at 4000 rpm for 1 minute. The samples were then placed in an oven at 110 °C for 1 hour. The resulting PEDOT:PSS film was 50 nm in thickness, as measured using a stylus profiler (*KLA Tencor*). The PEDOT:PSS covered ITO substrates were then transferred to a nitrogen-filled glove box.

The precursor solution for the lead iodide perovskite consisted of a 3:1 molar ratio of methylammonium iodide (2.4 M, *Ossila)* and lead (II) acetate (0.8 M, *Sigma-Aldrich*, 99.999%) in dimethyformamide (*Sigma-Aldrich*, 99.9%), prepared according to recent literature reports.[33,34] The solution was filtered through a PTFE syringe filter (0.2 µm, *VWR International*) and then spin-coated onto the ITO/PEDOT:PSS films for 2 minutes at different rotation speeds in order to tune the film thickness. As measured by a stylus profiler, the rotation speed of 1250 rpm, 1750 rpm, and 2500 rpm resulted in film thickness 450 nm, 300 nm, and 200 nm, respectively. The surface morphology of the 450-nm-thick film and 200-nm-thick film is shown in Figure S8 and highlight the polycristallinity of the $MAPbI_3$ layer whatever the thickness. The light yellow film obtained was then transferred onto a hot plate to be annealed at 90 °C for 25 minutes. During annealing, the color of the film slowly turned to dark brown, indicating the crystallization of lead iodide perovskite. All operations were performed in a nitrogen-filled glove box.

Device Fabrication and Characterization: For solar cell devices, a 50-nm thick phenyl-C_{61}-butyric acid methyl ester ($PC_{61}BM$) layer was deposited on top of the lead iodide perovskite layer (thickness 200 nm) by spin coating (2500 rpm, 1 minute) a solution of $PC_{61}BM$ dissolved in chlorobenzene (20 mg ml^{-1}, *Sigma Aldrich*, 99.8%) and stirred overnight at 50 °C before use. The top electrode (30 nm of calcium/70 nm of aluminum) was then thermally evaporated on top of the $PC_{61}BM$ layer under a vacuum of ~10^{-6} mbar. The dark and illuminated current–voltage curves were measured in a nitrogen-filled glove box using a *Keithley 2400* sourcemeter (scan rate ~0.1 V s^{-1} in forward and reverse). The AM1.5G illumination condition was simulated by using a *K.H.S. SolarCelltest- 575* solar simulator with AM1.5G filters set at 100 mW cm^{-2} with a calibrated radiometer (IL 1400BL).

For the tunneling current and electroluminescence experiments, a 70-nm thick gold layer was thermally evaporated on the lead iodide perovskite films to form a metal-semiconductor contact. The samples (ITO/PEDOT:PSS/$MAPbI_3$/Au) were loaded into a cryostat chamber connected to a glove box so that the sample can be transferred without being exposed to humidity or oxygen. Cooling to 10K was achieved using a closed cycle helium cryostat (*Advanced Research Systems*). At each temperature (as specified in the text), the chamber is stabilized for 10 minutes before the current−voltage measurement is taken.

Photoelectron Spectroscopy Measurements: X-ray photoelectron spectroscopy (XPS) and ultraviolet photoelectron spectroscopy (UPS) measurements were performed at the *HEISY-ORG* (Heidelberg integrated system for organic materials) facilities. A monochromatic Al Kα (photon energy= 1486.6 eV) provided the excitation source for XPS. In UPS, a gas discharge lamp operated with helium to achieve He-I emission (energy 21.22 eV) was used. A small bias of 2.5 eV was applied to the sample when recording the secondary electron cutoff. A *Phi VersaProbe II* spectrometer was used as the photoelectron energy analyzer, with Gaussian broadening of 0.35 eV and 0.13 eV for XPS and UPS, respectively.

Time of Flight measurements: A 532-nm laser (*Continuum Minilite*) with pulses < 7 ns was used to photogenerate charge carriers from the ITO side of the sample (ITO/PEDOT:PSS/$MAPbI_3$ (300 nm)/Au), with an applied bias voltage to separate the electron−hole pairs. The photocurrent was then monitored by a digital oscilloscope (*Tektronix*). From the large absorption coefficient of $MAPbI_3$ at the excitation wavelength, we estimate the absorption depth of 532-nm light in $MAPbI_3$ to be around 150 nm, making it possible to obtain the charge carrier mobility from the plateau of the photocurrent (Figure S7).

Conclusions

In this work, the electrical properties of hole transport in typical polycrystalline $MAPbI_3$ used in the fabrication of solar cell has been investigated by means of physical (XPS, UPS, X-ray diffraction) and electrical (*I–V*, *C–V*, EL, TOF) experiments and simulations at low temperature. In samples featuring an electron blocking gold electrode, an electroluminescence signal can still be measured at high field at temperatures as low as 10K, evidence of electron injection in the active layer. Detailed comparison between simulation and experiments have shown that simple tunneling through a triangular barrier (Fowler–Nordheim

Journal of Materials Chemistry A Accepted Manuscript

Please do not adjust margins

View Article Online
DOI: 10.1039/C6TA08979H

Published on 26 October 2016. Downloaded by UNIVERSITE DE BORDEAUX on 26/10/2016 14:41:41.

tunneling) cannot explain the injection of electrons, suggesting the presence of strong band bending at the Au/$MAPbI_3$ interface. As this band bending cannot be the consequence of residual doping or ion accumulation, it has been attributed to an excess of hole acceptor traps localized at this interface. Further comparison between SCLC simulations including both volume and interface traps have confirmed this assumption, allowing us to extract both hole mobility ~ 10^{-4} cm^2 V^{-1} s^{-1} (in agreement with TOF experiments), volume shallow trap density ~ 10^{16} cm^{-3} (in agreement with previously reported values) and interface traps (in concentration up to 5×10^{19} cm^{-3}). These results provide essential information regarding the role of volume and interface defects in state-of-the-art hybrid perovskite semiconductors, such as those typically used in perovskite solar cells. The occurrence of trapping has to be taken into account for the conception and simulation of perovskite based devices.

Acknowledgements

The French National Research Agency (ANR) through the LabEx AMADEus (ANR-10- LABX-0042-AMADEUS through grant ANR-10-IDEX-0003-02 and ANR-10-EQPX-28-01/Equipex ELOR- PrintTec) has funded this work. We also acknowledge financial support from the Spanish Ministry of Economy and Competitiveness (MINECO) via the Unidad de Excelencia María de Maeztu MDM-2015-0538, MAT2014-55200 and PCIN-2015-255.

Notes and references

[1]A. Kojima, K. Teshima,, Y. Shirai, T. Miyasaka, *J. Am. Chem. Soc.* 2009**, 131**, 6050.
[2]M. Saliba, T. Matsui, J.-Y. Seo, K. Domanski, J.-P. Correa-Baena, M. K. Nazeeruddin, S. M. Zakeeruddin, W. Tress, A. Abate, A. Hagfeldt, and M. Gratzel, *Energy Environ. Sci.* 2016, **9**, 1989.
[3]W.-J. Yin, T. Shi, and Y. Yan, *Appl. Phys. Lett.* 2014, **104**, 063903.
[4]a) S. D. Stranks, G. E. Eperon, G. Grancini, C. Menelaou, M. J. P. Alcocer, T. Leijtens, L. M. Herz, A. Petrozza, H. J. Snaith, *Science* 2013, **342**, 341. b) G. Xing, N. Mathews, S. Sun, S. S. Lim, Y. M. Lam, M. Grätzel, S. Mhaisalkar, T. C. Sum, *Science* 2013, **342**, 344.
[5]S. De Wolf, J. Holovsky, S.-J. Moon, P. Löper, B. Niesen, M. Ledinsky, F.-J. Haug, J.-H. Yum, C. Ballif, *J. Phys. Chem. Lett.* 2014, **5**, 1035.
[6]Y. Tian, A. Merdasa, M. Peter, M. Abdellah, K. Zheng, C. S. Ponseca Jr., T. Pullerits, A. Yartsev, V. Sundström, I. G. Scheblykin, *Nano Lett*. 2015, **15**, 1603.
[7]X. Wen, Y. Feng, S. Huang, F. Huang, Y.-B. Cheng, M. Green, A. Ho-Baillie *J. Mater. Chem. C* 2016, **4**, 793.
[8]X. Wu, M. T. Trinh, D. Niesner, H. Zhu, Z. Norman, J. S. Owen, O. Yaffe, B. J. Kudisch, X.-Y. Zhu, *J. Am. Chem. Soc.* 2015, **137**, 2089.
[9]T. M. Brenner, D. A. Egger, L. Kronik, G. Hodes, D. Cahen, *Nat. Rev. Mater.* 2016, **1**, 15007.
[10]N. Huby, L. Hirsch, L. Aubouy, P. Gerbier, A. Van Der Lee, F. Amy, A. Kahn, *Phys. Rev. B* 2007, **75**, 115416.
[11]J. Endres, D. A. Egger, M. Kulbak, R. A. Kerner, L. Zhao, S. H. Silver, G. Hodes, B. P. Rand, D. Cahen, L. Kronik, and A. Kahn, *J. Phys. Chem. Lett.* 2016, **7**, 2722.
[12]A. Miyata, A. Mitioglu, P. Plochocka, O. Portugall, J. T.-W. Wang, S. D. Stranks, H. J. Snaith, R. J. Nicholas, *Nat. Phys.* 2015**, 11**, 582.
[13]M. B. Price, J. Butkus, T. C. Jellicoe, A. Sadhanala, A. Briane, J. E. Halpert, K. Broch, J. M. Hodgkiss, R. H. Friend, F. Deschler, *Nat. Commun.* 2015, **6**, 8420.
[14]G. Giorgi, J. I. Fujisawa, H. Segawa, K. Yamashita, *J. Phys. Chem. Lett.* **2013**, 4, 4213.
[15]P. Umari, E. Mosconi, F. De Angelis, *Sci. Rep.* **2014**, 4, 4467.
[16]E. Menendez-Proupin, P. Palacios, P. Wahnon, J. C. Conesa, *Phys. Rev. B* **2014,** 90, 045207.
[17]G. Giorgi, K. Yamashita, *J. Mater. Chem. A* 2015, **3**, 8981.
[18]J. Feng, B. J. Xiao, *Phys. Chem. Lett.* 2014, **5**, 1278.
[19]C. Motta, F. El-Mellouhi, S. Sanvito, *Sci. Rep.* 2015, **5**, 12746.
[20] M. Hirasawa, T. Ishihara, T. Goto, K. Uchida, and N. Miura, *Phys. B Condens. Matter*. 1994, **201**, 427.
[21] V. D'Innocenzo, G. Grancini, M. J. P. Alcocer, A. R. S. Kandada, S. D. Stranks, M. M. Lee, G. Lanzani, H. J. Snaith, and A. Petrozza, *Nat. Commun.* 2014, **5**, 3586.
[22]D. Bryant, S. Wheeler, B. C. O'Regan, T. Watson, P. R. F. Barnes, D. Worsley, J. Durrant, *J. Phys. Chem. Lett.* 2015, **6**, 3190.
[23]M. Bag, L. A. Renna, R. Y. Adhikari, S. Karak, F. Liu, P. M. Lahti, T. P. Russell, M. T. Tuominen, D. Venkataraman, *J. Am. Chem. Soc.* 2015, **137**, 13130.
[24]J. G. Labram, D. H. Fabini, E. E. Perry, A. J. Lehner, H. Wang, A. M. Glaudell, G. Wu, H. Evans, D. Buck, R. Cotta, L. Echegoyen, F. Wudl, R. Seshadri, M. L. Chabinyc, *J. Phys. Chem. Lett.* 2015, **6**, 3565.
[25]J. H. Heo, H. J. Han, D. Kim, T. K. Ahn, S. H. Im, *Energy Environ. Sci.* 2015**, 8**, 1602.
[26]C.-H. Chiang, C.-G.Wu, *Nat. Phot.* 2016, **10**, 196.
[27]W. Franz, in *Handbuch der Physik*, Vol. 17 (Ed: S. Flugge), Springer, Berlin, Germany **1956**, p. 206ff.
[28]A. Lampert, P. Mark, *Current Injection in Solids*, Academic Press, New York, USA **1970**.
[29]T. Minemoto, M. Murata, *J. Appl. Phys.* 2014, **116**, 054505.
[30]C. Wehrenfennig, G. E, Eperon, M. B. Johnston, H. J. Snaith, L. M. Herz, *Adv. Mater.* 2014, **26**, 1584.
[31]B. Maynard, Q. Long, E. A. Schiff, M. Yang, K. Zhu, R. Kottokkaran, H. Abbas, V. L. Dalal, *Appl. Phys. Lett.* 2016, **108**, 173505.
[32]Y. Chen, J. Peng, D. Su, X. Chen, Z. Liang, *ACS Appl. Mater. Interfaces* 2015, **7**, 4471.
[33]D. Forgács, M. Sessoloa, H. J. Bolink, *J. Mater. Chem. A* 2015**, 3**, 14121.
[34]W. Zhang, M. Saliba, D. T. Moore, S. K. Pathak, M. T. Hörantner, T. Stergiopoulos, S. D. Stranks, G. E. Eperon, J. A. Alexander-Webber, A. Abate, A. Sadhanala, S. Yao, Y. Chen, R. H. Friend, L. A. Estroff, U. Wiesner, H. J. Snaith, *Nat. Commun.* 2015, **6**, 6142.

Journal of Materials Chemistry A Accepted Manuscript

Please do not adjust margins